Decreased Dissolution of ZnO by Iron Doping Yields Nanoparticles with Reduced Toxicity in the Rodent Lung and Zebrafish Embryos

Tian Xia,[†,#] Yan Zhao,[‡,#] Tina Sager,[§,#] Saji George,[†] Suman Pokhrel,[⊥] Ning Li,[†] David Schoenfeld,[‡] Huan Meng,[†] Sijie Lin,[†] Xiang Wang,[†] Meiying Wang,[†] Zhaoxia Ji,[¶] Jeffrey I. Zink,[∥,¶] Lutz Mädler,[⊥,¶] Vincent Castranova,[§] Shuo Lin,[‡] and Andre E. Nel[†,¶,*]

[†]Division of NanoMedicine, Department of Medicine, [‡]Department of Molecular, Cell and Developmental Biology, University of California, Los Angeles, California 90095, United States, [§]National Institute for Occupational Safety and Health, Morgantown, West Virginia 26506, United States, [⊥]Foundation Institute of Materials Science, Division of Process & Chemical Engineering, Department of Production Engineering, University of Bremen, Germany, [∥]Department of Chemistry & Biochemistry, University of California, Los Angeles, California 90095, United States, and [¶]California NanoSystems Institute, University of California, Los Angeles, California 90095, United States. [#] These authors contributed equally to this work.

ABSTRACT We have recently shown that the dissolution of ZnO nanoparticles and Zn^{2+} shedding leads to a series of sublethal and lethal toxicological responses at the cellular level that can be alleviated by iron doping. Iron doping changes the particle matrix and slows the rate of particle dissolution. To determine whether iron doping of ZnO also leads to lesser toxic effects *in vivo*, toxicity studies were performed in rodent and zebrafish models. First, we synthesized a fresh batch of ZnO nanoparticles doped with 1−10 wt % of Fe. These particles were extensively characterized to confirm their doping status, reduced rate of dissolution in an exposure medium, and reduced toxicity in a cellular screen. Subsequent studies compared the effects of undoped to doped particles in the rat lung, mouse lung, and the zebrafish embryo. The zebrafish studies looked at embryo hatching and mortality rates as well as the generation of morphological defects, while the endpoints in the rodent lung included an assessment of inflammatory cell infiltrates, LDH release, and cytokine levels in the bronchoalveolar lavage fluid. Iron doping, similar to the effect of the metal chelator, DTPA, interfered in the inhibitory effects of Zn^{2+} on zebrafish hatching. In the oropharyngeal aspiration model in the mouse, iron doping was associated with decreased polymorphonuclear cell counts and IL-6 mRNA production. Doped particles also elicited decreased heme oxygenase 1 expression in the murine lung. In the intratracheal instillation studies in the rat, Fe doping was associated with decreased polymorphonuclear cell counts, LDH, and albumin levels. All considered, the above data show that Fe doping is a possible safe design strategy for preventing ZnO toxicity in animals and the environment.

KEYWORDS: ZnO · dissolution · pulmonary toxicity · iron doping · zebrafish embryo · mouse · rat

We have previously demonstrated that nano-ZnO exerts toxicity in mammalian cells as a result of particle dissolution in the tissue culture medium as well as intracellularly.[1,2] Zn^{2+} shedding during intracellular dissolution induces lysosomal damage, $[Ca^{2+}]_i$ flux, mitochondrial perturbation, generation of reactive oxygen species (ROS), excitation of pro-inflammatory responses, and cell death.[1,2] We have also shown that altering the ZnO matrix through Fe doping decreases particle dissolution in tissue culture media, leading to a reduction in toxicological responses using a rapid throughput screening assay that includes the above response parameters.[1] The key question now is whether the reduced toxicity *in vitro* is also reflected by a reduction of toxicity in the lungs of rodents, which are known to exhibit pro-inflammatory effects to ZnO as well as in zebrafish, where this material interferes in embryo hatching.[3,4] The use of pulmonary inflammation as a basis for tracking *in vivo* ZnO toxicity in rodents is relevant to an occupational exposure condition in humans that is also characterized by acute inflammation.[5−7] Metal fume fever (MFF) develops in welders as a result of inadvertent exposure to ZnO and other metal oxide fumes.[5−7] The condition is characterized by high fever and pulmonary symptoms due to acute cytokine and chemokine (*e.g.*, IL-8, IL-6, and TNF-α) generation in the lung, leading to acute inflammation.[5,6,8] This is similar to the acute increase of TNF-α and IL-6 seen in mice and rats after acute ZnO exposure.[9,10]

Consideration of the environmental impact of ZnO is also becoming more relevant in light of the high use volume of this material in consumer products such as sunscreen products that could make their way to the environment *via* wastewater systems.[11] Nano-ZnO has been classified as "extremely toxic" in the environment.[11] Although we do not know how much engineered ZnO nanoparticles gain access to the environment, it is important to develop relevant environmental models and sentinel species that can be used to screen for

*Address correspondence to anel@mednet.ucla.edu.

Received for review October 22, 2010 and accepted January 7, 2011.

Published online January 20, 2011
10.1021/nn1028482

© 2011 American Chemical Society

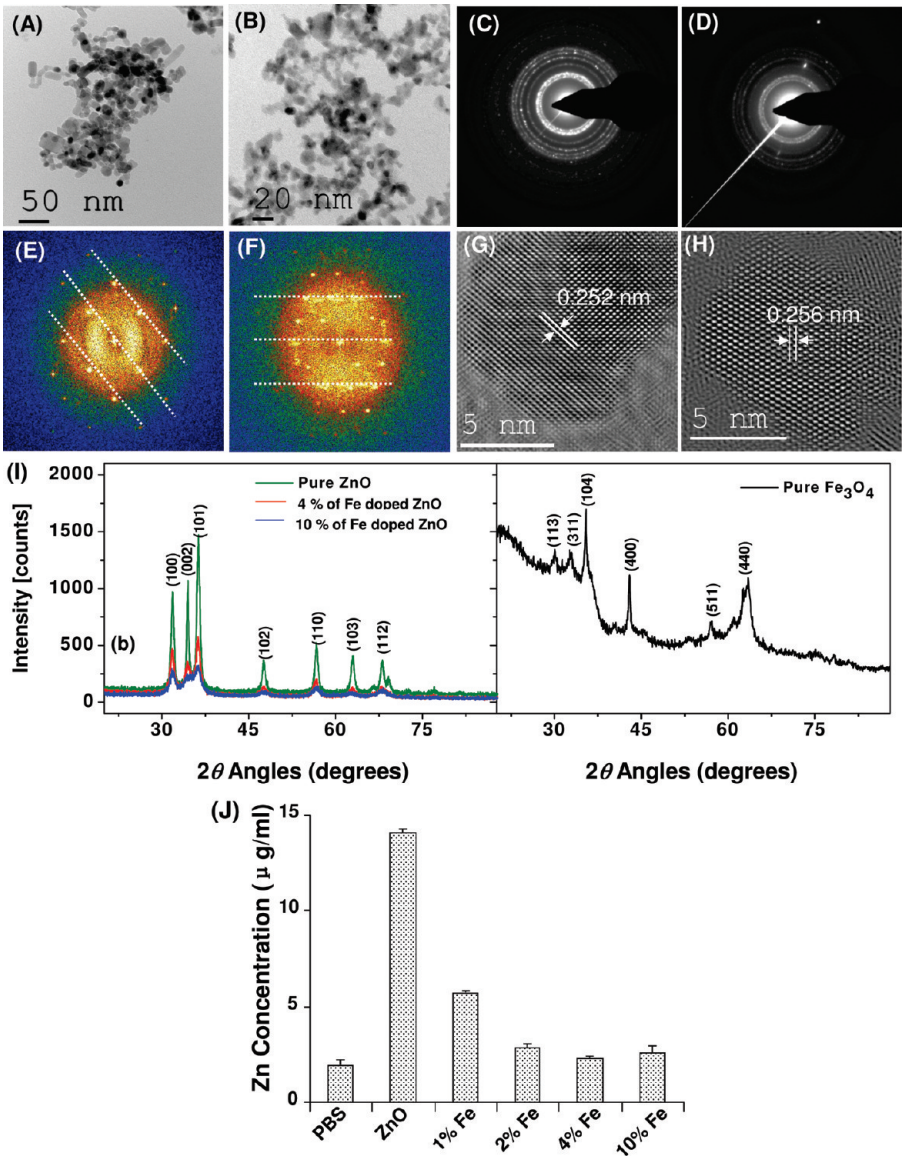

Figure 1. Physicochemical characterization to determine the effect of iron doping on ZnO nanoparticle matrix characteristics. Low-resolution TEM was used to assess the size and shape of undoped ZnO (A) and 10.2 wt % Fe-doped ZnO (B). SAED patterns were used to show the high crystallinity of pure ZnO (C) and 10.2 wt % Fe-doped ZnO (D). Power spectrum of single crystalline pure (E) and 10.2 wt % Fe-doped ZnO nanoparticles (F). High-resolution TEM images of the pure ZnO (G) and 10.2 wt % Fe-doped ZnO NPs (H) show that there is no difference in the lattice spacings, phase segregation, or formation of separate iron oxide particles. (I) Representative X-ray diffraction (XRD) patterns were used to confirm the crystalline structures of undoped and Fe-doped ZnO NPs. The X-ray patterns of pure Fe_3O_4 particles were obtained using Mo Kα source. The XRD patterns of Fe_3O_4 do not match the 10 wt % Fe-doped ZnO nanoparticles, suggesting homogeneous distribution of the Fe in the ZnO lattice. (J) Effect of Fe doping on ZnO dissolution was determined by ICP-MS: 50 μg/mL nanoparticles was suspended in PBS at room temperature in the presence of DPPC and BSA for 48 h. The suspension was centrifuged at 20,000*g* for 1 h, and the zinc concentration in the supernatant was determined by ICP-MS.

possible ZnO toxicity in this setting. Zebrafish have proven quite useful for environmental toxicity screening and are also useful for comparative biology because of the similarities between the zebrafish and human genomes, early life development, and disease processes.[11−14] Moreover, compared with more costly and time-consuming rodent models, screening of zebrafish embryos is inexpensive and can theoretically be used for high-throughput data collection.[13] Several studies reported that nano-ZnO induces interference in hatching, a decreased survival rate, tissue damage, and morphological abnormalities in zebrafish embryos.[3,4] Moreover, this toxicity is dependent on particle dissolution and shedding of Zn ions, which differs from the impact of soluble Zn.[3,4]

In spite of the considerable research into the potential hazardous effects of ZnO nanoparticles under biological conditions, no deliberate attempts have been made to design a potentially safer material that is less soluble. To study whether iron doping could decrease the toxicity of nano-ZnO in zebrafish, mouse, and rat models, we determined whether Fe-doped ZnO has an effect on the survival, hatching, or morphological features of zebrafish

TABLE 1. Surface Area and Primary Particle Size through BET Measurements

NPs	surface area (m^2/g)	BET equivalent particle size (nm)
ZnO	52	20.2
ZnO + 1% Fe	69	15.4
ZnO + 2% Fe	76	13.9
ZnO + 4% Fe	92	11.4
ZnO + 6% Fe	130	8.1
ZnO + 8% Fe	128	8.2
ZnO + 10% Fe	126	8.3
Fe_3O_4	143	8

embryos. We also assessed the effects of oropharyngeal and intratracheal instillation of undoped and doped particles in mouse and rat studies that were performed as a collaborative effort between two participating laboratories in a U.S. consortium using standardized laboratory protocols for each species to investigate batches of well-characterized ENMs. Our findings demonstrate that Fe doping leads to improved hatching rates in zebrafish embryos as well as decreased pulmonary inflammation in rodents. If proven not to interfere with the commercial use properties of ZnO, iron doping could be considered as a safe design strategy for this material.

RESULTS

Synthesis and Characterization of Iron-Doped ZnO Nanoparticle Library. We and others have previously demonstrated that the toxicological effects of ZnO particles have an important relationship with particle dissolution, which starts in the tissue culture or environmental medium and continues inside cells as well as possibly in the tissues and organs of intact organisms.[2−4,9,15,16] We hypothesized that a decrease in Zn^{2+} shedding could lead to a decrease in nano-ZnO cytotoxicity and demonstrated in a rapid throughput screening assay that iron doping can slow particle dissolution to improve the cytotoxicity profile.[1] A key question now becomes whether the doped particles also exhibit increased safety features *in vivo*. To address this question, we synthesized a fresh batch of undoped as well as Fe-doped ZnO nanoparticles that include 1.02, 2.02, 4.09, 6.1, 8.2, and 10.2 atomic weight % of iron. Low-resolution transmission electron microscopy (TEM) (Figure 1A,B) and Brunauer−Emmett−Teller (BET) analysis (Table 1) demonstrate that doping yields somewhat smaller spherical particles (8.3−15 nm) compared to the undoped particles (20.2 nm). This size reduction is due to compression stress and the smaller ionic radius of Fe (Zn^{2+} = 0.074 nm, Fe^{3+} = 0.0645 nm).[17,18] Selected area diffraction patterns (SAED) (Figure 1C,D) and power spectrum (Figure 1E,F) analyses further confirmed that up to 10.2 wt % iron doping is possible without changing lattice spacings, phase segregation, or yielding separate iron oxide particles. Moreover, Fourier transformed high-resolution TEM pictures to study the hexagonal arrangement of the lattices show that Fe doping has no influence on the high degree of crystallinity of the ZnO matrix (Figure 1G,H). This was further confirmed by the demonstration that the lattice distances of the undoped (0.252 nm) and doped (0.256 nm) particles were not significantly different. This finding is further supported by the X-ray diffraction (XRD) patterns of undoped and doped particles (Figure 1I).

We have previously shown that iron doping affects ZnO nanoparticle dissolution in water and tissue culture medium.[1] In order to determine whether iron doping exerts similar effects in phosphate buffered saline (PBS), 50 μg of the undoped and doped particles was added to 1 mL of PBS in the presence of dipalmitoylphosphatidylcholine (DPPC) and bovine serum albumin (BSA) at room temperature. BSA and DPPC are used for particle dispersal in pulmonary instillation studies because they are naturally present in lung lining fluid.[19] The supernatant of the centrifuged particle suspension in PBS was collected after 48 h for inductively coupled plasma mass spectrometry (ICP-MS) analysis, which demonstrated a decrease in Zn release proportional to the level of doping (Figure 1J). An iron doping level of 4 wt % restored the [Zn] in the supernatant to near background levels.

Iron doping affects the surface properties of the nanoparticles in water, PBS, and Holtfreter's solution (Table 2). Holtfreter's solution is used as a substitute environmental medium for zebrafish embryo studies. Iron doping above 4 wt % leads to a decrease in ZnO nanoparticle zeta-potential due to the effect of Fe_3O_4 on the particle surface. This, in turn, leads to decreased electrostatic repulsion and increased aggregation as demonstrated by the increased hydrodynamic radii of the doped particles (Table 2). However, the addition of DPPC and BSA decreased the agglomerate size, likely as a result of coating the particles' surfaces (Table 2).[16] Use of alginate to stabilize the particles in Holtfreter's solution (Materials and Methods) also leads to a decrease in agglomerate size but increases the negative zeta-potential of the particles (Table 2). Alginate is an environmentally relevant dispersant that is used for studying the ecotoxicological effects of nanomaterials[20] similar to the use of BSA and DPPC as stabilizing agents for pulmonary studies.

Confirming the Biological Efficacy of Iron Doping with Our Cellular Screening Assay. In order to confirm that the new batch of undoped and doped nanoparticles indeed exhibit differential toxicity profiles, we compared their abilities in an *in vitro* screening assay that was previously developed to assess sublethal and lethal toxicological responses in RAW 264.7 and BEAS-2B cells.[1] This assay screens for mitochondrial superoxide production (MitoSox red), $[Ca^{2+}]_i$ flux (Fluo-4), mitochondrial depolarization (JC-1), and plasma membrane leakage (PI).[1] Details of this recently published multiparametric screening assay are delineated in more detail in Materials and Methods as well as the Supporting Information.[1] Three hours following the addition of the particles and tracking the sublethal and lethal response readouts by an automated epifluorescence procedure, the data were used to construct a

TABLE 2. Size, Polydispersity Index, and Zeta-Potential of Iron-Doped ZnO[a]

	water		PBS		PBS + DPPC and BSA		Holtfreter		Holtfreter + alginate	
NPs	size (nm)	PDI	size (nm)	PDI	size (nm)	PDI	size (nm)	PDI	size (nm)	PDI
ZnO	158 ± 10	0.086	817 ± 143	0.017	804 ± 45	0.015	889 ± 214	0.101	379 ± 2	0.044
1% Fe−ZnO	160 ± 11	0.110	1316 ± 193	0.015	505 ± 12	0.006	1336 ± 214	0.217	236 ± 11	0.071
2% Fe−ZnO	193 ± 65	0.105	1108 ± 169	0.051	460 ± 73	0.018	1147 ± 150	0.210	242 ± 14	0.031
4% Fe−ZnO	462 ± 129	0.031	845 ± 72	0.037	579 ± 118	0.015	966 ± 159	0.048	411 ± 44	0.107
10% Fe−ZnO	1297 ± 215	0.112	1146 ± 86	0.010	367 ± 57	0.020	946 ± 39	0.029	717 ± 118	0.031
Fe_3O_4	142 ± 15	0.230	998 ± 142	0.013	170 ± 10	0.010	1372 ± 87	0.075	229 ± 2	0.046

	zeta-potential (mV)				
NPs	water	PBS	PBS + DPPC and BSA	Holtfreter	Holtfreter + alginate
ZnO	14.3 ± 1.1	−16.4 ± 0.8	−15.8 ± 1.6	−15.1 ± 1.3	−40.2 ± 0.9
ZnO + 1% Fe	21.2 ± 0.7	−35.9 ± 2.7	−17.1 ± 2.1	−11.1 ± 1.4	−38.0 ± 1.6
ZnO + 2% Fe	20.8 ± 1.5	−36.8 ± 3.7	−18.4 ± 3.1	−12.5 ± 0.8	−37.9 ± 1.4
ZnO + 4% Fe	10.5 ± 1.3[b]	−31.8 ± 3.2	−15.7 ± 2.9	−15.9 ± 1.3	−34.3 ± 1.1
ZnO + 10% Fe	2.8 ± 3.2[b]	−27.1 ± 3.3	−19.7 ± 1.7	−19.6 ± 2.1	−36.6 ± 2.5
Fe_3O_4	−24.5 ± 5.2[b]	−28.5 ± 4.4	−18.1 ± 2.4	−19.6 ± 1.7	−33.2 ± 3.3

[a] Particle size in solution was determined by high-throughput dynamic light scattering (HT-DLS, Dynapro Plate Reader, Wyatt Tech). Nanoparticle size was expressed as intensity-based average hydrodynamic diameter ± SE. Zeta-potential was expressed as mean ± SE ($n = 5$). PDI = Polydispersity index. Particle zeta-potential in solution was measured by ZetaPALS (Brookhaven Instruments, Holtsville, NY). [b] Compared to ZnO, $p < 0.05$.

heatmap in which the green−red color display reflects the fold increase in fluorescence intensity in nanoparticle-exposed compared to control cells (Supporting Information Figure S1). Compared to undoped particles, Fe-doped ZnO revealed a progressive decline in all of the toxicological responses in accordance with the Fe doping levels (Supporting Information Figure S1). The protective effect was more pronounced in RAW 264.7 than in BEAS-2B cells, as previously demonstrated.[2] In summary, *in vitro* toxicological profiling confirmed that iron doping leads to protective cellular effects. Please notice that for the purposes of this study the *in vitro* assay is used as a biological tool to confirm the efficiency of iron doping and was not included for extrapolation to *in vivo* studies.

Iron Doping Interferes in the Inhibition of Zebrafish Embryo Hatching by ZnO Nanoparticles. The zebrafish represents an appropriate environmental organism for studying the effects of ZnO nanoparticles, which is regarded as extremely toxic in the environment.[11] Not only does the zebrafish embryo constitute an *in vivo* model that can be used for rapid throughput screening but it is also appropriate for comparison to mammalian biological responses.[12,13] First, we monitored the morphological changes during embryo development in the 5−120 hours post fertilization (hpf) time frame. This analysis showed that undoped ZnO nanoparticles interfere in embryo hatching without directly affecting viability (Figure 2A). However, hatching failure ultimately leads to the starvation and death of the live embryos.

The hatching of fish embryos is facilitated by hatching enzymes that are produced by a hatching gland embedded in the chorionic sac. Previous studies have shown that the ZHE1 is a major zebrafish hatching enzyme (ZHE) being secreted into the chorionic fluid by the gland and plays a major role in digesting the interior aspect of the chorionic membrane.[21,22] In order to test the possible effect of Zn on ZHE1 production, we performed whole mount *in situ* hybridization (ISH) to determine ZHE1 expression in the intact embryo. ISH was performed by employing RNA probes against ZHE1 mRNA.[23] Visual inspection of the ISH product did not show any change in the staining intensity of the hatching gland in embryos exposed to ZnO (Supporting Information Figure S2). Since this result was also confirmed by real-time PCR that showed no effect on ZHE1 mRNA levels (not shown), we addressed a possible effect on ZHE1 enzyme activity. Because a quantitative ZHE assay is not available, we used an indirect biological approach for assessing enzyme activity by visualizing digestion of the chorionic membrane. Figure 2B shows that the intact zebrafish chorion at 4 hpf comprises a thin, dark exterior layer (the result of osmium tetroxide staining) as well as a thicker interior layer that exhibits porous indentations 500−700 nm in diameter.[24] Under normal hatching conditions, both the interior and exterior layers are digested away within 48 hpf at the weaker pore sites. However, in the presence of ZnO nanoparticles, the chorionic membrane remained intact up to 120 hpf, suggesting a loss of hatching enzyme activity (Figure 2B and Supporting Information Figure S3).

In order to more definitively demonstrate that the rate of ZnO dissolution is important in hatching interference, we examined the effect of Fe doping and metal chelation on embryo hatching. First, we performed a dose−response study to determine the optimal ZnO dose to use (Supporting Information Figure S4) and decided to use

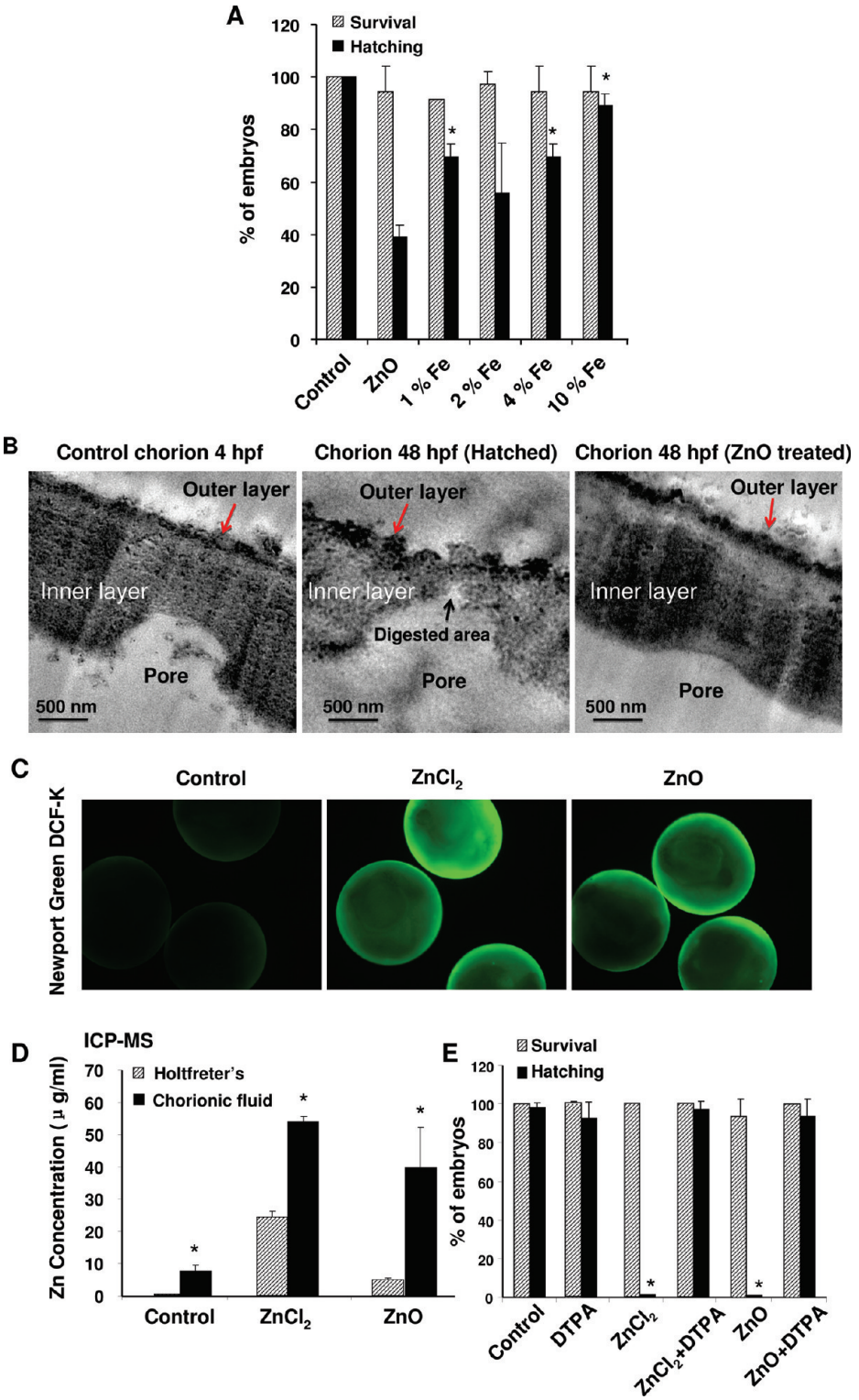

Figure 2. Effects of iron doping on zebrafish embryo hatching and Zn uptake in the chorion. (A) Effects of iron-doped NPs on the survival and hatching rate of zebrafish embryos were observed at 120 hpf (5 μg/mL, 36 embryos/group); *$p < 0.05$ compared with embryos treated with undoped particles. (B) TEM of zebrafish chorions with or without ZnO treatment (20 μg/mL, 48 hpf). (C) Fluorescent images taken after microinjection of Newport Green DCF-K (500 μM) in zebrafish embryos exposed to 50 μg/mL of $ZnCl_2$ or ZnO nanoparticles for 24 h. Fluorescent images of the embryos were taken under a fluorescent microscope. Eighteen embryos were imaged in each treatment group. (D) ICP-MS analysis to determinate Zn concentrations in the chorionic fluid extracted from embryos or present in Holtfreter's solution that received 50 μg/mL of $ZnCl_2$ or ZnO nanoparticles for 24 h. Fifty embryos were examined in each group in duplicates; *$p < 0.05$ compared with Holtfreter's solution. (E) Effects of chelator DTPA, 100 μM for 72 h, on hatching and survival rate of zebrafish embryos exposed to 10 μg/mL of $ZnCl_2$ or ZnO nanoparticles for 72 h; *$p < 0.05$ compared with corresponding groups supplemented with DTPA.

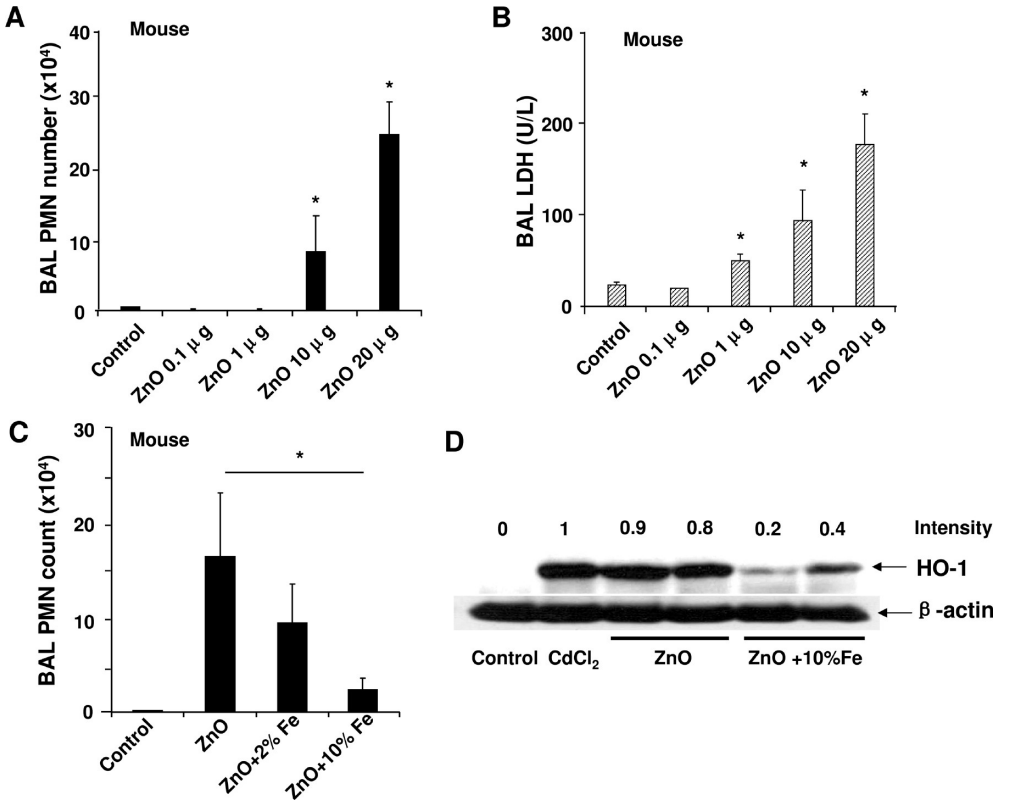

Figure 3. Dose-dependent pulmonary inflammation in mice and the effects of Fe doping on ZnO toxicity. (A) PMN numbers in BAL fluid 40 h after the oropharyngeal aspiration of incremental doses of ZnO nanoparticles in C57BL6 mice (6 mice/group). (B) LDH activity in the BAL fluid of the same exposed animals as in (A); *$p < 0.05$ compared with control. (C) PMN cell counts in BAL fluid collected after 40 h exposure to 20 μg undoped or 2 and 10 wt % Fe-doped nanoparticles. The experiment was repeated twice; *$p < 0.05$ compared with control. (D) Western blot looking at HO-1 and β-actin expression in two mouse lungs each for animals exposed to either undoped or 10 wt % Fe-doped ZnO nanoparticles. A mouse treated with $CdCl_2$ by oropharyngeal exposure served as the positive control.

5 μg/mL for comparative studies. This demonstrated a significant improvement in hatching rate with incremental levels of Fe doping, with near normal hatching at a 10 wt % doping level (Figure 2A). Because this suggests that Zn is critical for hatching interference, we microinjected the Zn-specific fluorescent dye, Newport Green DCF-K, into the chorionic sac to see if $ZnCl_2$ or ZnO affects the dye's fluorescence intensity. Indeed, both the soluble as well as particulate form of ZnO induced a visible increase in green fluorescence intensity (Figure 2C). To quantitatively assess this increase in the [Zn] in the chorionic fluid, some of the fluid was withdrawn and analyzed by ICP-MS. This demonstrated that, compared to the surrounding medium, there is a significant increase in the [Zn] in the fluid (Figure 2D). Moreover, the incremental jump in [Zn] for ZnO nanoparticles (8-fold) was more than that of soluble $ZnCl_2$ (2-fold). In order to confirm the doping results, we also conducted a study of the effect of the metal chelator, diethylenetriaminepentaacetic acid (DTPA), on embryo hatching and survival. The data show that DTPA was capable of interfering in the inhibitory effects of $ZnCl_2$ and ZnO nanoparticles (Figure 2E). Taken together, these results demonstrate the dissolution characteristics of ZnO nanoparticles play a key role in this material's toxicity in zebrafish embryos.

Iron Doping Leads to Reduced ZnO Pulmonary Inflammation in the Mouse. The assessment of pulmonary toxicity is a valid platform for *in vivo* toxicity assessment of ZnO nanoparticles based on the finding that both human and rodent exposures lead to acute pulmonary inflammation.[5−8,15,25,26] It was decided to use both rats and mice since two of the participating laboratories in this study are part of a U.S. consortium that uses a standardized oropharyngeal aspiration protocol in mice and a standardized intratracheal instillation protocol in rats to do comparative studies on common batches of engineered nanomaterials (ENMs). We used oropharyngeal aspiration of undoped ZnO to establish an initial dose−response study in the lung of C57BL/6 mice (Figure 3A,B). This demonstrated incremental increases in the polymorphonuclear cell (PMN) count and lactate dehydrogenase (LDH) levels in the bronchoalveolar lavage (BAL) fluid over the dose range of 1−20 μg of ZnO per animal (Figure 3A,B). Twenty micrograms was used in subsequent studies to compare undoped with 2 and 10 wt % Fe-doped ZnO nanoparticles. While 2 wt % doping lowered the acute inflammatory response, the results became statistically significant at 10 wt % doping (Figure 3C). The reduction in PMN cell counts in the BAL fluid was accompanied

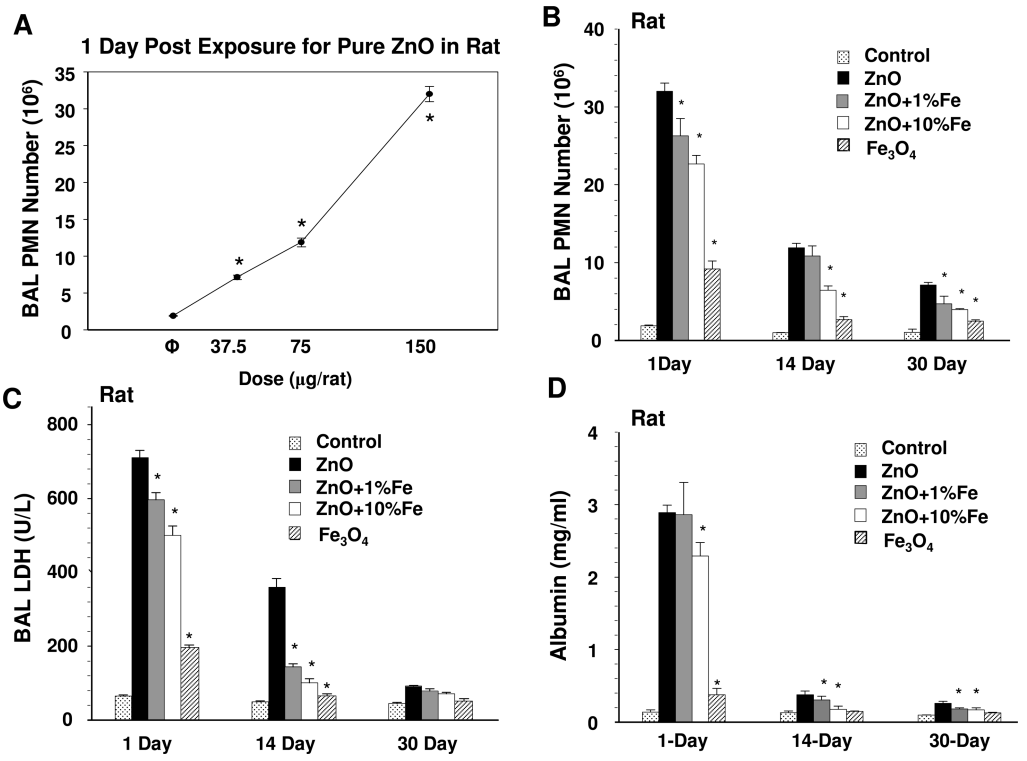

Figure 4. Dose-dependent pulmonary inflammation in rats and the effects of Fe doping on ZnO toxicity. Rats (8 animals per group) were exposed to undoped or doped ZnO particles *via* intratracheal instillation (IT). Each animal received a dose of 150 μg of ZnO particles dispersed in PBS with BSA plus DPPC. At 24 h, 14 days, and 30 days post-instillation, the animals were euthanized and BAL fluid was collected to determine PMN numbers, LDH, and albumin levels. The experiment was repeated twice; *$p < 0.05$ compared with control (A) and ZnO-treated rats (B, C, D).

by a reduction in IL-6 mRNA levels in the lungs of animals receiving particles doped with 10 wt % Fe (Supporting Information Figure S5). Because ZnO cytotoxicity[1,2] (Supporting Information Figure S1) as well as the pro-inflammatory effects on welding fumes in boilermakers is accompanied by oxidative stress responses,[8] heme oxygenase 1 (HO-1) expression was used as an oxidative stress biomarker in the lungs of animals receiving undoped and 10 wt % doped particles. The Western blot in Figure 3D shows reduced HO-1 expression in both animals receiving doped particles. Interestingly, the pro-inflammatory effects in the BAL fluid were not accompanied by histological abnormalities in the lungs of the exposed mice, which is in keeping with the absence of permanent structural abnormalities in the lungs of humans with MFF.[5,27]

Iron Doping of ZnO Leads to Reduced Pulmonary Inflammation in the Rat. We also used undoped and Fe-doped ZnO nanoparticles to study the effects in rats receiving these materials intratracheally. While similar to mice, rats show acute pulmonary inflammation,[25] there are quantitative and qualitative differences. Rats exhibit more severe and persistent pulmonary inflammation in response to nanoparticles than mice, including the potential to develop progressive fibroproliferative lesions.[28] Doses of 37.5, 75, and 150 μg were administered intratracheal in male Sprague-Dawley rats, which were sacrificed at 1, 14, and 30 days postexposure to assess BAL PMN counts, LDH activity, and albumin levels. The undoped ZnO nanoparticles produced a dose-dependent increase in PMN cell counts in the BAL fluid at 24 h (Figure 4A). Also, the respective doses of Fe-doped nano-ZnO caused a significant increase in PMN over controls at all postexposure time periods (Figure 4B). While for both the undoped as well as the Fe-doped nano-ZnO, the influx of PMNs into the lung decreased over a 30 day observation period, PMN levels remained significantly higher than control PMN levels at all concentrations and at all observation periods (Figure 4B). Even though the PMN levels remained significantly elevated for the Fe-doped particles, doping did have a significant reduction on PMN levels compared to that caused by the undoped particles. For instance, at the highest administered dose (150 μg/rat), PMN levels were significantly decreased with 1 and 10 wt % Fe doping levels at the 24 h observation period (Figure 4B). Only the 10 wt % Fe-doped particles were capable of lowering the PMN responses to a 150 μg particle dose at the 14 and 30 day observation periods (Figure 4B). LDH levels in BAL fluid after treatment with 1 and 10 wt % Fe-doped ZnO were significantly decreased after 1 and 14 days compared to undoped particles (Figure 4C). Albumin levels after treatment of 10 wt % Fe-doped ZnO decreased significantly after 1, 14, and 30 days treatment compared to undoped particles, while albumin levels were

significantly decreased in response to 1 wt % Fe-doped ZnO after 14 and 30 days treatment (Figure 4D). Iron doping showed similar protective effects at lower exposure amounts (75 and 37.5 μg/rat) compared to undoped particles (not shown). All considered, the rodent studies showed similar as well as complementary response outcomes that support a protective pulmonary effect through iron doping.

DISCUSSION

In this study, we explored the effect of iron doping ZnO nanoparticles in three different animal models to determine whether the improvement of cellular toxicity is also accompanied by reduction of *in vivo* health effects in zebrafish embryos and the rodent lung. While in zebrafish Fe doping prevented interference in embryo hatching, the principal effects in the mouse and rat lungs were to decrease acute pulmonary inflammation and cytotoxicity. All considered, these data demonstrate that ZnO toxicity in rodents and the environment can be reduced by iron doping.

The demonstration that Fe doping leads to decreased *in vitro* and *in vivo* toxicity indicates that safe-by-design strategies are possible for engineered nanomaterials. As a first step of such a strategy, we demonstrate the importance of identifying the major material characteristics that are responsible for the toxicity, through the use of proof-of-principle testing. For ZnO, dissolution and shedding of zinc ions play an important role in its toxicity. However, it is unclear at this stage whether specific surface area or surface reactivity also plays a role in its toxicity. The second key step is to develop a strategy to change, alter, or eliminate the hazardous property, which for ZnO could mean slowing its dissolution by Fe doping. The iron in the ZnO lattice can be found in both oxidation states (Fe^{2+} and Fe^{3+}). The theoretical calculations suggest that the stability of the Fe^{2+} in the ZnO lattice is relatively larger compared to that for Fe^{3+}, and these two oxidation states have a coupling constant of 1.4 eV as evidenced from electron energy loss spectroscopy (EELS) spectra.[29] Due to the stable dopants present in the ZnO lattice, the dissolution of the doped particles is reduced compared to that of undoped particles. Although it is still too early to evaluate the commercial impact of such a strategy for nano-ZnO application in the marketplace, it is useful to consider the real-life scenarios where Fe doping may be helpful to reduce toxicity in humans and the environment. While it is not possible to introduce doping during welding, we should consider the scenario of ZnO being used in skin care products, particularly commercial sunscreens where this material is used to absorb UV light. While there has been considerable debate as to whether nano-ZnO poses any danger on the skin, most studies have demonstrated that these nanoparticles do not penetrate the skin. However, a recent study using a ZnO sunscreen prepared from Zn^{68} demonstrated that very small quantities of Zn can penetrate the protective layers of human skin with the potential to generate small increases in the isotope levels in blood and urine.[30] While there is no evidence that this is clinically harmful, it is important from an environmental perspective to consider that ZnO nanoparticles being washed from the skin have the potential to spread to the environment *via* wastewater systems. Although the actual level of environmental contamination by ZnO is currently unknown, Kaegi *et al.* have provided a quantitative assessment of the amounts of TiO_2 nanoparticles that can gain access to the aquatic environment through runoff.[31] They estimated that the concentration of TiO_2 nanoparticles in the runoff collected from beneath the facades is as high as 0.55 μg/mL.[31] This compares favorably to the starting dose of 1 μg/mL ZnO that was used in our zebrafish studies. Moreover, if we consider the 8-fold bioconcentration in the chorionic sac (Figure 2C,D), the toxicological relevant levels in the environment could be even lower. In a recent report by Kahru *et al.*, the median $L(E)C_{50}$ value for nano-ZnO in fish was estimated to be 2 μg/mL.[11] Nano-ZnO was classified as "extremely toxic" to environmental organisms such as fish, bacteria, algae, crustaceans, ciliates, yeasts, and nematodes.[11] From the perspective that Fe doping could reduce ZnO toxicity by decreasing the Zn release to the environment, additional studies will be required once the technology becomes available to detect ZnO nanoparticles in the environment. Additional consideration should also be given to the possibility that decreasing the dissolution may allow the ZnO particles to remain intact for longer periods and may therefore spread to environmental targets that may have otherwise not been exposed to Zn. It is clear, therefore, that fate and transport studies are necessary to fully interpret the toxicity studies. Another practical consideration would be to determine whether doped ZnO nanoparticles maintain their desired functionality in the commercial products that incorporate ZnO nanoparticles. We know that ZnO maintains its ability for UV absorption following Fe doping.[32,33] Moreover, the band gap energy of the pure ZnO (3.3 eV) does not change much with doping levels up to 15%.[33] The band gap value for 4% Fe-doped ZnO is 3.22 eV, which is not significantly different than undoped ZnO.[32]

Comparison of *in vitro* and *in vivo* dosimetry remains a challenge in ENM toxicity but can be approached by normalizing the ZnO dose per surface area in the tissue culture dish and comparing that to the normalized surface area dose in the airways in mice and rats. Through the use of morphometry analysis, Stone *et al.* have estimated the alveolar epithelial area in the mouse, rat, and human to be 0.05, 0.4, and 102 m^2, respectively.[34] Therefore, exposure doses of 150 and 20 μg in the rat and mouse would normalize to 0.038 and 0.04 $\mu g/cm^2$, respectively. This is comparable to a human lung burden

of 40.8 mg. Assuming that the particles are evenly deposited across the tissue culture dish, this would amount to an *in vitro* surface area dose of 0.24−10 μg/cm^2. Thus, on a comparative basis, the *in vitro* doses used in our cellular screening assay were minimally an order of magnitude higher than the doses used in the rodent lung but do not take into consideration the possibility of uneven deposition in the conducting airways and the alveoli. This could have the effect of concentrating the particle dose at select airway generations as has been proven experimentally for different size particles.[35] Moreover, we have to consider that the higher *in vitro* exposure doses were applied for a relatively short (3 h) time period compared to the 24 h or longer exposure times in the rodent respiratory tract. Given the current shortcomings of performing *in vitro/in vivo* dose comparisons, it is not possible to make more accurate comparisons. Nonetheless, it is highly significant that iron doping exerted the same level of protective effect *in vivo* as it did in our *in vitro* studies. With this proof-of-principle demonstration, future studies will perform more direct comparison of *in vivo* and *in vitro* doses, including performance of aerosolized inhalation exposures that simulate real-life exposure conditions.

Our finding that nano-ZnO interferes in zebrafish hatching agrees with previous studies.[3,4] Although failure to hatch could eventually lead to the death of the embryo as a result of starvation, use of dechorionated embryos did not demonstrate any morphological defects or actual impact on survival, even at a dose as high as 50 μg/mL (not shown). These data suggest that the principal effect of nano-ZnO is interference in the function of ZHE1 and possibly other hatching enzymes. We further demonstrated that Zn is concentrated in the chorionic fluid, which could be the result of passive diffusion and the high osmotic pressure of the protein-rich fluid.[36] However, it is also possible that some of ZnO nanoparticles may be able to pass through the chorion pore canals.[24] These channels are as large as 0.5−0.7 μm in diameter and have been shown to allow Ag nanoparticles to enter the chorionic fluid.[24] At present, we are not able to differentiate between Zn in its ionic form or nanoparticulate form in the chorionic fluid. However, we showed that a metal chelator (DTPA) is capable of restoring embryo hatching during exposure to either an ionic zinc solution or ZnO nanoparticles. While we are aware of at least one other study showing that Zn^{2+} can accumulate in zebrafish embryos, that study did not attempt to assess the Zn concentrations in the chorionic fluid.[37] The possibility that the chorion is capable of concentrating Zn^{2+} or ZnO nanoparticles has important implications for a spectrum of fish embryos. In addition to zebrafish, trout, medaka, and minnow embryos have been shown to bioconcentrate heavy metals (*e.g.*, methyl Hg, Ag, Cd) and chemicals (*e.g.*, phenanthrene, atrazine).[38−40] However, we do not know whether ZnO nanoparticles interfere in the hatching of other embryos. In this regard, it is important to consider the differences in the functional properties of the chorion across fish species. Nonetheless, the zebrafish embryo could be very helpful as an *in vivo* model for developing a predictive toxicological paradigm in combination with cellular screening studies. It is also possible to perform high-throughput screening studies in zebrafish embryos.[13]

Previous studies in rats have shown that nano-ZnO particles are capable of inducing acute pulmonary inflammation, including neutrophil recruitment and LDH release in the BAL fluid.[26] ZnO exposures have also been shown to increase metallothionein and HO-1 gene expression in the rat lung, suggesting that oxidative stress plays a role in pulmonary inflammation.[25] Similar studies in mice have shown that nano-ZnO induces acute pulmonary inflammation that leads to PMN infiltration and increased protein content in the BAL fluid in parallel with metallothionein gene expression in the lung.[15,26] These findings are compatible with cellular screening[2] and the human studies showing that oxidative stress plays a role in the pro-inflammatory effects of ZnO in the lung.[2,5−8] Although dissolution of ZnO nanoparticles was previously implicated in the acute inflammatory effects of this material, most of the evidence was based on deductive reasoning, including the rapid recovery rate in MFF.[5−7,27] This communication provides the first direct evidence that decreased dissolution of ZnO by Fe doping can reduce pulmonary inflammation. However, as cautioned in the environmental studies, we should consider that slowing of particle dissolution is a double-edged sword that could under some circumstances pose new risks by being able to spread to sites that may not normally be accessed by dissolving ZnO nanoparticles. We demonstrate that the decreased pulmonary inflammation in response to the doped particles is accompanied by less HO-1 expression, suggesting a reduction in pulmonary oxidative stress. Oxidative stress may contribute to the activation of pro-inflammatory pathways that trigger the expression of cytokines and chemokines such as IL-6, TNF-α, and IL-8 in MFF.[5−7,27] It will be interesting in future studies to compare the dissolution rate of other nanoparticles that are capable of metal ion shedding and pulmonary toxicity, including Ag, Co, Cu and Ni nanoparticles.[41−43] However, different from the high dissolution rates of ZnO, most of these nanoparticles are less soluble and a key question therefore becomes to what extent the ion shedding is responsible for pulmonary toxicity compared to a reactive particle surface. We propose that our predictive toxicological platform that involves cellular injury pathways to interpret *in vivo* studies may help to generate the knowledge that is required for comprehensive assessment of ENM toxicity.[44]

The awareness of safe-by-design ENM approaches is now moving the nano-EHS (Environmental Health & Safety) field to consideration of proactive strategies at the design and development stage of new products rather than regarding EHS as a *postfacto* add-on or imposed cleanup cost.[44−46] An understanding of hazardous ENM properties is essential for safe design from a biological and environmental perspective. While there is no single design

feature that currently fits this description, possible approaches that might contribute to this area are being identified, and the current communication serves as a proof-of-principle study that now needs to be executed under real-life exposure conditions. It is important to note that a change in properties may affect ENM performance characteristics (*e.g.*, electrical conductivity, thermal conductivity, or magnetic properties) that are essential for technology or product development. Thus, while the potential impact on product performance must be properly explored, it is possible that certain compromises may have to be made.

CONCLUSION

We asked whether the ZnO nanoparticles doped with iron would improve the safety profile of this material in the zebrafish embryo and rodent lung. We demonstrate that doped particles exhibit a reduced rate of toxicity compared with undoped ZnO in all three animal models. While doping reduced the inhibitory effect of Zn on embryo hatching in zebrafish, the major effect in the lung was a reduction in pulmonary inflammation and oxidative stress response.

MATERIALS AND METHODS

Flame Spray Pyrolysis (FSP) Synthesis of Undoped and Fe-Doped ZnO NPs. The metallorganic precursors, zinc naphthenate (8% of Zn, Strem Chemical, 99.9% pure) and iron naphthenate (12% Fe, Strem Chemical, 99.9% pure), were used for the synthesis of undoped and Fe-doped ZnO nanoparticles. The synthesis of nanoparticles (undoped and Fe-doped) was based on atomic wt % of this metal (same as wt %). The calculation is wt % = {[weight of Fe precursor (6.5 mL, by Fe)]/[weight of Fe precursor (6.5 mL, Fe) + weight of 50 mL Zn precursor (by Zn)]} × 100. The densities of the undoped and Fe-doped ZnO nanoparticles are close to one another (ZnO has 5.6 g/cm^3 where as Fe_3O_4 has 5.1 g/cm^3). Briefly, a 50 mL portion of 0.5 M zinc naphthenate was separately mixed with 0.6−6.5 mL of 0.5 M iron naphthenate to provide 1−10 wt % of Fe doping. For undoped ZnO and Fe_3O_4, 50 mL of 0.5 M Zn or Fe precursors was separately used. All of the precursors were dissolved in an organic solvent (xylene, 99.95%, Strem) to keep the metal concentration at 0.5 M. Each liquid precursor was delivered to the nozzle tip by a syringe pump at a flow rate of 5 mL/min by atomizing the precursor solution with dispersant O_2 and maintaining a pressure drop of 1.5 bar at the nozzle tip. Combustion of the dispersed droplets is initiated by the co-delivery of CH_4 and O_2 (1.5 L/min, 3.2 L/min) to create a flame.

Physicochemical Characterization of Fe-Doped ZnO Nanoparticles. Surface area was determined by Brunauer−Emmett−Teller (BET), which measures N_2 adsorption−desorption on the particle surface. The measurements were carried out at 77 K using a Quantachrome NOVA 4000e Autosorb gas sorption system. The BET method was used to determine the specific surface area of the samples. The powders were placed in a test cell and allowed to degas for 2 h at 200 °C in flowing nitrogen. Data were obtained by introducing or removing a known quantity of adsorbing gas in or out of a sample cell containing the solid adsorbent maintained at a constant liquid nitrogen temperature.

The crystallinity of undoped and Fe-doped ZnO was determined by transmission electron microscopy (TEM). The FSP-generated metal oxide nanoparticles were sonicated in ethanol for 3 h before TEM analysis. The microscopic imaging of the specimens was investigated with a FEI Titan 80/300 microscope equipped with a Cs corrector for the objective lens, a Fischione high angle annular dark field detector (HAADF), a GATAN postcolumn imaging filter, and a cold field emission gun operated at 300 kV as an acceleration voltage. A Kevex energy-dispersive X-ray spectrometer was used at 10 eV per channel for power spectrum and SAED patterns. Spectra were taken at each sampling point to identify the homogeneity of the samples. X-ray diffraction (XRD) analysis of nanoparticles was performed in reflection mode on a PW 3040/60 X'Pert PRO diffractometer equipped with X'Celerator linear detector using a Cu Kα (λ = 0.154 nm) radiation and step size of 0.01° for the ZnO and Fe-doped ZnO NPs. The pure Fe_3O_4 NPs were placed in circular sample holders with a diameter of 16 mm and then loaded into a Bruker D8 diffracting system. The diffractometer was configured in Bragg-Brentano geometry, equipped with a primary Johansson monochromator producing pure Mo Kα1 (λ = 0.07093 nm) radiation. A ∼0.1° fixed divergence, 4° primary 2.5° secondary Soller slits, and LynxEye detector (position sensitive in a range of 3° 2θ with 192 channels, yielding a channel width of 0.01563° 2θ) was used. Continuous scans in the range of 5−55° 2θ were applied with an integration step width of ∼0.03° 2θ and 30 s per step.

Nanoparticle Dispersion in Cell Culture Media, Holtfreter's Solution, and PBS. Nanoparticle stock solutions (5 mg/mL) were prepared by dispersing the nanoparticle powder in deionized water by sonication (30 W). To ensure proper dispersion of nanoparticles, the stock solution was sonicated before removing aliquots to prepare fresh working solutions for each intended use condition. These included particle dispersion in tissue culture medium to perform cellular screening in Holtfreter's medium to study zebrafish embryos and in PBS to perform pulmonary exposure studies.

For tissue culture studies, the particles were precoated with bovine serum albumin (BSA) or fetal bovine serum (FBS) before transfer into BEGM or DMEM, respectively, as described.[1,16] The nanoparticles were suspended in the cell culture media by sonication (30 W) for 15 s prior to the addition to tissue culture plates.[16] The rationale and full explanation of this approach has recently been published by us.[1,16]

Holtfreter's solution contains 60 mM NaCl, 0.67 mM KCl, 2.4 mM $NaHCO_3$, and 0.8 mM $CaCl_2$ in deionized water at pH 6.5−7.1. In order to stabilize the particles in this ionic medium, alginic acid was used as a natural organic matter. This was accomplished by adding NPs dispersed in deionized water to Holtfreter's solution that was supplemented with 100 ppm alginic acid. The mixture was sonicated for 15 s at 30 W before dispensing the medium in tissue culture plates for the performance of zebrafish experiments.

For the performance of oropharyngeal aspiration or intratracheal instillation studies in mice and rats, respectively, particles were suspended in PBS in the presence of 0.6 mg/mL BSA plus 0.01 mg/mL dipalmitoylphosphatidylcholine (DPPC). DPPC was prepared fresh as a 10 mg/mL stock solution in absolute ethanol (200 proof). Each particle suspension was briefly sonicated before use.[19,47] The rationale for the use of this dispersal protocol has been previously published by us.[19,47]

Nanoparticle Size Distribution and Zeta-Potential Measurement. High-throughput dynamic light scattering (HT-DLS, Dynapro Plate Reader, Wyatt Technology) was performed for detecting the particles' state of aggregation/dispersion in water or tissue culture media in the absence or presence of dispersing agents (BSA + DPPC, FCS, or alginate).[16] The plate reader is operated similar to a traditional DLS instrument but with a more rapid readout that can be used for multiple particles being dispersed in a variety of different media. Since each measurement takes only a few seconds, it is possible to obtain 10 automated measurements for each sample loaded into triplicate wells of a 384-well plate. The data were collected with 158° back scattering. This approach is ideal for obtaining stable and well-dispersed particle suspensions and facilitates rapid throughput cytotoxicity screening. A ZetaPALS (Brookhaven Instruments, Holtsville, NY) instrument was used to determine the electrophoretic mobility from which zeta-potential

of the nanoparticles could be calculated by the Helmholtz–Smoluchowski equation.[48]

Inductively Coupled Plasma Mass Spectrometry (ICP-MS) Analysis. ICP-MS analysis was performed to detect zinc ion released from ZnO nanoparticles suspended in physiological media; 50 μg/mL nanoparticles was suspended in PBS at room temperature in the presence of DPPC and BSA for 48 h. The suspension was centrifuged at 20 000*g* for 1 h, and a 500 μL portion of supernatant was acidified with 500 μL of 7% ultrahigh purity nitric acid, and the zinc concentration was measured by a Perkin-Elmer SCIEX Elan DRCII.

Mammalian Cell Culture and Coincubation with Nanoparticles. All cell cultures were maintained in 25 cm^2 cell culture flasks, in which the cells were passaged at 70–80% confluency every 2–4 days. RAW 264.7 cells (ATCC# TIB71) were cultured in Dulbecco's modified Eagle medium (DMEM) (In Vitrogen, Carlsbad, USA) supplemented with 10% FBS, 100 U/mL penicillin, 100 μg/mL streptomycin, and 2 mM L-glutamine (complete medium). Five thousand cells were plated into each well of a 384-well plate (CellBound, Corning Inc., MA) for overnight culture at 37 °C in 5% CO_2 before nanoparticle addition. BEAS-2B (ATCC# CRL-9609) cells were cultured in BEGM (Lonza, San Diego, CA) in type-I rat tail collagen-coated flasks. Trypsinized cells were washed and plated at 5000 cells per well (0.06 cm^2) in 384-well plates before being cultured for 2 days in a 5% CO_2 incubator prior to nanoparticle treatment. Nanoparticles prior coated with BSA and then dispersed in complete DMEM or 2 mg/mL BSA in BEGM were used for RAW 264.7 and BEAS-2B exposures, respectively.

***In Vitro* Multiparametric Screening To Compare Cytotoxic Effects of Undoped and Doped ZnO Nanoparticles.** Three fluorescent dye cocktail mixtures were prepared by mixing wavelength-compatible fluorescent probes in phenol-red-free DMEM media as previously described.[1] Briefly, the first cocktail contained Hoechst 33342 (1 μM) and JC-1 (1 μM); the second cocktail contained Hoechst 33342 (1 μM), Fluo-4 (5 μM) and propidium iodide (5 μM), while the third cocktail contained Hoechst 33342 (1 μM) and MitoSox Red (5 μM). Several unique NP properties such as high adsorption capacity, optical properties, surface catalytic activity *etc*. can interfere with the fluorescence readout and may introduce artifacts. We addressed these issues by incorporating the necessary controls, including the addition of particles to dyes in the absence of cells, particles with cells but without the addition of dyes, and addition of dyes to cells in the absence of particles. The implementation procedures for performance of this multiparametric screening have been described in detail in a recent publication.[1] Each well of the 384-well plate received 50 μL of dye mixture for 30 min under standard (dark) cell culture conditions. Unincorporated dyes were removed by washing, following which tissue culture wells were replenished with phenol-red-free DMEM or BEGM. Cellular fluorescence imaging was acquired using an Image-Xpress^{micro} (Molecular Devices, Sunnyvale, CA) equipped with laser autofocus. DAPI, FITC, and TRITC filter/dichroic combinations were used to image Hoechst 33342 (blue), Fluo-4 (green), and PI (red), respectively. Images were processed using MetaXpress (Molecular Devices, Sunnyvale, CA). We used fluorescent intensity of the cells to calculate the fold increase over that of the untreated control cells. The data were displayed as a heatmap. The red and warmer colors in the heatmap are indicative of a higher fold increase in toxicity, while the green shows little or no toxic effects. It should also be noted that *in vitro* cell lines are substantially different from cells under *in vivo* environment. The cells used in this study (mouse leukemic monocytes and human bronchial epithelial cells) are proliferating, undifferentiated, and submersed cell lines, while lung epithelial cells and the surface macrophages *in vivo* are highly differentiated cells that grow at the air–liquid interface and have a low turnover. So care must be taken to interpret *in vitro* cell line results.

Exposure of Zebrafish Embryos to Nanoparticles. Wild-type AB line of zebrafish stocks were obtained from the Zebrafish International Resource Stock Center (ZIRC) (Oregon) and maintained in the UCLA zebrafish core facility as described.[43] Only healthy female and male zebrafish were selected for generation of the embryos. A healthy female fish typically generates 200–300 embryos. After fertilization, the embryos were collected and rinsed several time in Holtfreter's solution to remove any residue on the embryo surface. The embryos were examined under a stereomicroscope for health and developmental state (32–64 cell stage) according to an established protocol that only utilizes healthy embryos that are plated 1 embryo per well in 96-well plates. At 4–6 h post-fertilization (~1000 cell stage), the embryos were re-examined before nanoparticle treatment. The Holtfreter's solution was drained with a pipet and replaced at 4–6 hpf with 100 μL of the same solution containing the nanoparticle suspensions. The embryos were observed *via* a Zeiss Stemi 2000-C dissection microscope every 24 h for 5 days in order to assess hatching rate, embryo mortality, and morphological abnormalities (large/small yolk size, yolk sac edema, no blood circulation, lack of pigmentation, body length, curved body axis, delayed eye/head development, opaque necrotic tissue, and pericardial edema).

TEM of Zebrafish Chorions. Chorions from wild-type zebrafish embryos at 4 hpf, naturally hatched embryos at 48 hpf, and ZnO treated embryos at 48 hpf were collected for fixing (50 embryos per group). Initial fixing was performed with 0.1 M sodium cacodylate buffer, pH 7.4, containing 4% paraformaldehyde and 1% glutaraldehyde for 2 h. Secondary fixing was done in 1% OsO_4 (also prepared in 0.1 M cacodylate buffer) for 1 h on ice. Samples were dehydrated through a gradient of ethanol solution after fixation. After dehydration, chorion samples were embedded in SPURR resin and allowed to polymerize overnight at 60 °C. Thin sectioning (70 nm) was performed using a Leica Ultratome, and TEM images were captured at 120 kV using a Philips CM120 microscope.

Analysis of Zebrafish Hatching Enzyme (ZHE1) Gene Expression by Real-Time PCR and *In Situ* Hybridization (ISH). Both real-time PCR and whole-mount ISH were performed to examine the expression of ZHE1 gene in control and ZnO-treated zebrafish embryos. For real-time PCR, a total of 50 embryos per group were collected at 10, 24, and 48 hpf and homogenized in 1 mL of TRIZOL reagent (Invitrogen). Subsequently, 2 μg of total RNA was reverse transcribed by Superscript III reverse transcriptase (Invitrogen). cDNA was amplified by real-time PCR using SYBR Green Supermix (BioRad) and the following primers (ZHE1f 5′-ctgaacttctctacacactgagg-3′, ZHE1 r 5′-ccttatcaccatcacctcacttc-3′). Relative gene expression levels were reported as fold-change (FC) using the $\Delta\Delta C_t$ method where FC = 2-$\Delta\Delta$Ct.[49] For whole-mount ISH, a total of 40 embryos per group were collected at 10, 24, and 48 hpf, fixed with 4% paraformaldehyde in PBST and subsequently processed following the procedures described previously.[23]

Mouse Exposure and Assessment of Exposure Outcomes in Mice. Ten-week-old C57Bl/6NCrl mice were purchased from Charles River Laboratories (Hollister, CA). All animals were housed under standard laboratory conditions that have been set up strictly following UCLA guidelines for care and treatment of laboratory animals and the NIH Guide for the Care and Use of Laboratory Animals in Research (DHEW78-23). These conditions are approved by the Chancellor's Animal Research Committee at UCLA. These include detailed standard operating procedures for animal housing (filter-topped cages; room temperature at 23 ± 2 °C; 60% relative humidity; 12 h light, 12 h dark cycle) and hygiene status (autoclaved food and acidified water). Animal exposure to undoped and doped ZnO nanoparticles was carried out by an oropharyngeal aspiration method as previously described.[50] Briefly, the mice were anesthetized by intraperitoneal injection of ketamine (100 mg/kg)/xylazine (10 mg/kg) in a total volume of 100 μL. While the animals were held in a vertical position, a 50 μL suspension containing 0.1–20 μg undoped or Fe-doped ZnO nanoparticles was instilled at the back of the tongue to allow pulmonary aspiration. The control animals received the same volume of PBS without particles. Animals were euthanized by i.p. injection of 50 mg/kg pentobarbital. One milliliter of saline was used to lavage the lung, with the recovery of 0.8–0.85 mL of BAL fluid. The lungs were fixed by inflation with formalin. Lung sections were stained with hematoxylin and eosin for assessing neutrophilic inflammation as previously described by us.[51] The BALF was used for performance of total and differential cell count. LDH activity was assessed by using CytoTox 96 non-radioactive cytotoxicity assay

kit. Lung tissue was used for histology, HO-1 western blotting, and assessment of mRNA production.

Analysis of Gene Expression in the Mouse Lung by Real-Time PCR. To assess IL-6 mRNA expression, small lung pieces were harvested and placed in RNA Later (Qiagen, Valencia, CA). Lung tissues were homogenized in lysis buffer (Buffer RLT) containing β-mercaptoethanol with a 5 mm rotor-sator homogenizer (PRO Scientific, Oxford, CT). Total RNA was isolated using RNeasy Mini Kit according to manufacturer's instructions. Quantitative gene expression analysis was performed using procedures described above in the analysis of ZHE1 gene expression by real-time PCR. Statistical differences between $\Delta\Delta C_t$ values between groups were statistically determined with 2-way ANOVA (SigmaStat Ashburn, VA; $p \leq 0.05$).

Rat Exposure and Assessment of Exposure Outcomes. Male Sprague-Dawley (Hla: (SD) CVF) rats of approximate age of 10 weeks old and weighing 200−300 g were obtained from Hilltop Lab Animals (Scottdale, PA). The animals were housed in an AAALAC-accredited, specific pathogen-free, environmentally controlled facility at NIOSH. The animals were monitored to be free of endogenous viral pathogens, parasites, mycoplasms, *Helicobacter*, and CAR *Bacillus*. Animals were housed in ventilated cages receiving HEPA-filtered air, with Alpha-Dri virgin cellulose chips and hardwood Beta-chips used as bedding. The rats were maintained on a ProLaB 3500 diet and tap water, both of which were provided *ad libitum*. Rats were exposed to the undoped or doped ZnO nanoparticles *via* intratracheal instillation (IT). Animals were lightly anesthetized by an intraperitoneal (i.p.) injection of 30−40 mg/kg sodium methohexital (Brevital, Eli Lilly and Company, Indianapolis, IN). The animals were intratracheally instilled with 0.30 mL of undoped ZnO, 1 or 10% Fe-doped ZnO or Fe_3O_4 particles suspended in PBS containing BSA and DPPC using a 20 guage 4 in. ball tipped animal feeding needle.[19]

At 24 h, 14 days, and 30 days, the instilled animals were euthanized with an i.p. injection of sodium pentobarbital (>100 mg/kg body weight) and exsangainated by cutting the descending aorta. A tracheal cannula was inserted, and BAL was conducted.[19] A 6 mL aliquot of cold Ca^{2+}- and Mg^{2+}-free PBS was used for the first lavage wash. The cold PBS was flushed into and out of the lungs two times before BALF was collected. After the first lavage was collected, the BAL continued with 8 mL aliquots of cold Ca^{2+}- and Mg^{2+}-free PBS until an additional 80 mL of BALF was collected. The BALF from all rats was placed in a centrifuge at 600*g* for 10 min using a Sorvall RC 3B Plus centrifuge (Sorvall Thermo Electron Corporation, Asheville, NC). After centrifugation, the supernatant from the first lavage wash was decanted into a clean conical vial and was stored on ice to be used for cytotoxicity analysis. The remaining lavage wash supernatant was discarded, and the cells remaining were washed with cold Ca^{2+}- and Mg^{2+}-free PBS and spun again at 600*g* for 10 min. After this, the supernatant was discarded and the cells were resuspended in 1 mL of HEPES buffer. Using these lavage samples, polymorphonuclear neutrophil (PMN) and alveolar macrophage (AM) cell counts were performed using an electronic cell counter (Beckman Coulter Multisizer 3 Counter, Hialeah, FL). The degree of cytotoxicity induced by the instilled particles was determined by lactate dehydrogenase (LDH) activity in the BAL fluid. LDH activity was measured using Roche COBAS MIRA Plus chemical analyzer (Roche Diagnostic Systems Inc., Branchburg, NJ) as described previously by our laboratory.[19]

Statistics. Statistical differences between control and treatment groups for the *in vivo* experiments comparing the toxicity of the various ZnO particles were determined using an analysis of variance (ANOVA) with significance set at $p \leq 0.05$. Individual mean values were compared using the Student−Newman−Keuls method multiple comparison procedure with an overall significance level of 0.05.

Acknowledgment. This work is supported by the National Science Foundation and the Environmental Protection Agency under Cooperative Agreement Number DBI-0830117. Any opinions, findings, conclusions or recommendations expressed herein are those of the authors and do not necessarily reflect the views of the National Science Foundation, the Environmental Protection Agency, or the National Institute for Occupational Safety and Health. This work has not been subjected to an EPA peer and policy review. Key support was provided by the U.S. Public Health Service Grants, U19 ES019528 (UCLA Center for NanoBiology and Predictive Toxicology), RC2 ES018766, RO1 CA133697, and RO1 ES016746. Fluorescent microscopy was performed at the CNSI Advanced Light Microscopy/Spectroscopy Shared Facility at UCLA. Authors S.P. and L.M. would like to thank Dr. Johannes Birkenstock, Central Laboratory for Crystallography and Applied Materials, University of Bremen, Germany, for the XRD measurements. We also gratefully acknowledge Dr. Andreas Rosenauer, Department of Physics, University of Bremen, Germany, for the TEM measurements.

Supporting Information Available: Additional figures depicting hazard ranking by a heatmap, zebrafish whole mount *in situ* hybridization, additional TEM of zebrafish chorions, dose−response of iron doping on zebrafish embryo hatching and survival, and effects of iron doping on cytokine production in the lungs of mice were described in the text. This material is available free of charge *via* the Internet at http://pubs.acs.org.

REFERENCES AND NOTES

1. George, S.; Pokhrel, S.; Xia, T.; Gilbert, B.; Ji, Z.; Schowalter, M.; Rosenauer, A.; Damoiseaux, R.; Bradley, K. A.; Madler, L.; *et al.* Use of a Rapid Cytotoxicity Screening Approach To Engineer a Safer Zinc Oxide Nanoparticle through Iron Doping. *ACS Nano* **2010,** *4*, 15–29.
2. Xia, T.; Kovochich, M.; Liong, M.; Madler, L.; Gilbert, B.; Shi, H.; Yeh, J. I.; Zink, J. I.; Nel, A. E. Comparison of the Mechanism of Toxicity of Zinc Oxide and Cerium Oxide Nanoparticles Based on Dissolution and Oxidative Stress Properties. *ACS Nano* **2008,** *2*, 2121–2134.
3. Bai, W.; Zhang, Z.; Tian, W.; He, X.; Ma, Y.; Zhao, Y.; Chai, Z. Toxicity of Zinc Oxide Nanoparticles to Zebrafish Embryo: A Physicochemical Study of Toxicity Mechanism. *J. Nanopart. Res.* **2010,** *12*, 1645–1654.
4. Zhu, X.; Wang, J.; Zhang, X.; Chang, Y.; Chen, Y. The Impact of ZnO Nanoparticle Aggregates on the Embryonic Development of Zebrafish (*Danio rerio*). *Nanotechnology* **2009,** *20*, 195103.
5. Gordon, T.; Fine, J. M. Metal Fume Fever. *Occup. Med.* **1993,** *8*, 504–517.
6. Martin, C. J.; Le, X. C.; Guidotti, T. L.; Yalcin, S.; Chum, E.; Audette, R. J.; Liang, C.; Yuan, B.; Zhang, X.; Wu, J. Zinc Exposure in Chinese Foundry Workers. *Am. J. Ind. Med.* **1999,** *35*, 574–580.
7. Rohrs, L. C. Metal-Fume Fever from Inhaling Zinc Oxide. *AMA Arch. Ind. Health* **1957,** *16*, 42–47.
8. Wang, Z.; Neuburg, D.; Li, C.; Su, L.; Kim, J. Y.; Chen, J. C.; Christiani, D. C. Global Gene Expression Profiling in Whole-Blood Samples from Individuals Exposed to Metal Fumes. *Environ. Health Perspect.* **2005,** *113*, 233–241.
9. ATSDR Toxicological Profile for Zinc; U.S. Department of Health and Human Services, Public Health Service, Agency for Toxic Substances and Disease Registry, 2005.
10. Wesselkamper, S. C.; Chen, L. C.; Gordon, T. Quantitative Trait Analysis of the Development of Pulmonary Tolerance to Inhaled Zinc Oxide in Mice. *Respir. Res.* **2005,** *6*, 73.
11. Kahru, A.; Dubourguier, H. C. From Ecotoxicology to Nanoecotoxicology. *Toxicology* **2010,** *269*, 105–119.
12. Fako, V. E.; Furgeson, D. Y. Zebrafish as a Correlative and Predictive Model for Assessing Biomaterial Nanotoxicity. *Adv. Drug Delivery Rev.* **2009,** *61*, 478–486.
13. Zon, L. I.; Peterson, R. T. *In Vivo* Drug Discovery in the Zebrafish. *Nat. Rev. Drug Discovery* **2005,** *4*, 35–44.
14. Kari, G.; Rodeck, U.; Dicker, A. P. Zebrafish: An Emerging Model System for Human Disease and Drug Discovery. *Clin. Pharmacol. Ther.* **2007,** *82*, 70–80.
15. Wesselkamper, S. C.; Chen, L. C.; Gordon, T. Development of Pulmonary Tolerance in Mice Exposed to Zinc Oxide Fumes. *Toxicol. Sci.* **2001,** *60*, 144–151.
16. Ji, Z.; Jin, X.; George, S.; Xia, T.; Meng, H.; Wang, X.; Suarez, E.; Zhang, H.; Hoek, E. M.; Godwin, H.; *et al.* Dispersion and Stability Optimization of TiO_2 Nanoparticles in Cell Culture Media. *Environ. Sci. Technol.* **2010,** *44*, 7309–7314.

17. Height, M. J.; Madler, L.; Pratsinic, S. E. Nanorods of ZnO Made by Flame Spray Pyrolysis. *Chem. Mater.* **2006,** *18*, 572–578.
18. Toeh, W. Y.; Amal, R.; Madler, L.; Pratsinic, S. E. Flame Sprayed Visible Light-Active Fe-TiO_2 for Photomineralisation of Oxalic Acid. *Catal. Today* **2007,** *120*, 203–213.
19. Porter, D. W.; Sriram, K.; Wolfarth, M.; Jefferson, A.; Schwegler-Berry, D. E.; Andrew, M.; Castranova, V. A Biocompatible Medium for Nanoparticle Dispersion. *Nanotoxicology* **2008,** *2*, 144–154.
20. Chen, K. L.; Mylon, S. E.; Elimelech, M. Aggregation Kinetics of Alginate-Coated Hematite Nanoparticles in Monovalent and Divalent Electrolytes. *Environ. Sci. Technol.* **2006,** *40*, 1516–1523.
21. Okada, A.; Sano, K.; Nagata, K.; Yasumasu, S.; Ohtsuka, J.; Yamamura, A.; Kubota, K.; Iuchi, I.; Tanokura, M. Crystal Structure of Zebrafish Hatching Enzyme 1 From the Zebrafish *Danio rerio*. *J. Mol. Biol.* **2010,** *402*, 865–878.
22. Sano, K.; Inohaya, K.; Kawaguchi, M.; Yoshizaki, N.; Iuchi, I.; Yasumasu, S. Purification and Characterization of Zebrafish Hatching Enzyme—An Evolutionary Aspect of the Mechanism of Egg Envelope Digestion. *FEBS J.* **2008,** *275*, 5934–5946.
23. Kim, H. J.; Sumanas, S.; Palencia-Desai, S.; Dong, Y.; Chen, J. N.; Lin, S. Genetic Analysis of Early Endocrine Pancreas Formation in Zebrafish. *Mol. Endocrinol.* **2006,** *20*, 194–203.
24. Lee, K. J.; Nallathamby, P. D.; Browning, L. M.; Osgood, C. J.; Xu, X. H. *In Vivo* Imaging of Transport and Biocompatibility of Single Silver Nanoparticles in Early Development of Zebrafish Embryos. *ACS Nano* **2007,** *1*, 133–143.
25. Cosma, G.; Fulton, H.; DeFeo, T.; Gordon, T. Rat Lung Metallothionein and Heme Oxygenase Gene Expression Following Ozone and Zinc Oxide exposure. *Toxicol. Appl. Pharmacol.* **1992,** *117*, 75–80.
26. Sayes, C. M.; Reed, K. L.; Warheit, D. B. Assessing Toxicity of Fine and Nanoparticles: Comparing *In Vitro* Measurements to *In Vivo* Pulmonary Toxicity Profiles. *Toxicol. Sci.* **2007,** *97*, 163–180.
27. Fine, J. M.; Gordon, T.; Chen, L. C.; Kinney, P.; Falcone, G.; Beckett, W. S. Metal Fume Fever: Characterization of Clinical and Plasma IL-6 Responses in Controlled Human Exposures to Zinc Oxide Fume at and below the Threshold Limit Value. *J. Occup. Environ. Med.* **1997,** *39*, 722–726.
28. Bermudez, E.; Mangum, J. B.; Asgharian, B.; Wong, B. A.; Reverdy, E. E.; Janszen, D. B.; Hext, P. M.; Warheit, D. B.; Everitt, J. I. Long-Term Pulmonary Responses of Three Laboratory Rodent Species to Subchronic Inhalation of Pigmentary Titanium Dioxide Particles. *Toxicol. Sci.* **2002,** *70*, 86–97.
29. Benzerara, K.; Yoon, T. H.; Menguy, N.; Tyliszczak, T.; Brown, G. E., Jr. Nanoscale Environments Associated with Bioweathering of a Mg-Fe-Pyroxene. *Proc. Natl. Acad. Sci. U.S.A.* **2005,** *102*, 979–982.
30. Gulson, B.; McCall, M.; Korsch, M.; Gomez, L.; Casey, P.; Oytam, Y.; Taylor, A.; Kinsley, L.; Greenoak, G. Small Amounts of Zinc from Zinc Oxide Particles in Sunscreens Applied Outdoors Are Absorbed through Human Skin. *Toxicol. Sci.* **2010,** *118*, 140–149.
31. Kaegi, R.; Ulrich, A.; Sinnet, B.; Vonbank, R.; Wichser, A.; Zuleeg, S.; Simmler, H.; Brunner, S.; Vonmont, H.; Burkhardt, M.;*et al.*Synthetic TiO_2 Nanoparticle Emission from Exterior Facades into the Aquatic Environment. *Environ. Pollut.* **2008,** *156*, 233–239.
32. Chen, A. J.; Wu, X. M.; Sha, Z. D.; Zhuge, L. J.; Meng, Y. D. Structure and Photoluminescence Properties of Fe-Doped ZnO Thin Films. *J. Phys. D: Appl. Phys.* **2006,** *39*, 4762–4765.
33. Wang, C. Z.; Chen, Z.; He, Y.; Li, L.; Zhang, D. Structure, Morphology and Properties of Fe-Doped ZnO Films Prepared by Facing-Target Magnetron Sputtering System. *Appl. Surf. Sci.* **2009,** *255*, 6881–6887.
34. Stone, K. C.; Mercer, R. R.; Gehr, P.; Stockstill, B.; Crapo, J. D. Allometric Relationships of Cell Numbers and Size in the Mammalian Lung. *Am. J. Respir. Cell Mol. Biol.* **1992,** *6*, 235–243.
35. Phalen, R. F.; Oldham, M. J.; Nel, A. E. Tracheobronchial Particle Dose Considerations for *In Vitro* Toxicology Studies. *Toxicol. Sci.* **2006,** *92*, 126–132.
36. Eddy, F. B. Osmotic Properties of the Perivitelline Fluid and Some Properties of the Chorion of Atlantic Salmon Eggs (*Salmo salar*). *J. Zool., London* **1974,** *174*, 237–243.
37. Mages, M.; Bandow, N.; Kuster, E.; Brack, W.; von Tumpling, W. Zinc and Cadmium Accumulation in Single Zebrafish (*Danio rerio*) Embryos—A Total Reflection X-ray Fluorescence Spectrometry Application. *Spectrochim. Acta, Part B* **2008,** *63*, 1443–1449.
38. Schreiber, R.; Altenburger, R.; Paschke, A.; Schuurmann, G.; Kuster, E. A Novel *In Vitro* System for the Determination of Bioconcentration Factors and the Internal Dose in Zebrafish (*Danio rerio*) Eggs. *Chemosphere* **2009,** *77*, 928–933.
39. de Wolf, W.; Comber, M.; Douben, P.; Gimeno, S.; Holt, M.; Leonard, M.; Lillicrap, A.; Sijm, D.; van Egmond, R.; Weisbrod, A.;*et al.*Animal Use Replacement, Reduction, and Refinement: Development of an Integrated Testing Strategy for Bioconcentration of Chemicals in Fish. *Integr. Environ. Assess Manag.* **2007,** *3*, 3–17.
40. Lacoue-Labarthe, T.; Warnau, M.; Oberhansli, F.; Teyssie, J. L.; Koueta, N.; Bustamante, P. Differential Bioaccumulation Behaviour of Ag and Cd during the Early Development of the Cuttlefish Sepia Officinalis. *Aquat. Toxicol.* **2008,** *86*, 437–446.
41. Duffin, R.; Tran, L.; Brown, D.; Stone, V.; Donaldson, K. Proinflammogenic Effects of Low-Toxicity and Metal Nanoparticles *In Vivo* and *In Vitro*: Highlighting the Role of Particle Surface Area and Surface Reactivity. *Inhal. Toxicol.* **2007,** *19*, 849–856.
42. Fubini, B. Surface Reactivity in the Pathogenic Response to Particulates. *Environ. Health Perspect.* **1997,** *105*, 1013–1020.
43. Warheit, D. B.; Webb, T. R.; Colvin, V. L.; Reed, K. L.; Sayes, C. M. Pulmonary Bioassay Studies with Nanoscale and Fine-Quartz Particles in Rats: Toxicity Is Not Dependent upon Particle Size but on Surface Characteristics. *Toxicol. Sci.* **2007,** *95*, 270–280.
44. Meng, H.; Xia, T.; George, S.; Nel, A. E. A Predictive Toxicological Paradigm for the Safety Assessment of Nanomaterials. *ACS Nano* **2009,** *3*, 1620–1627.
45. Hutchison, J. E. Greener Nanoscience: A Proactive Approach to Advancing Applications and Reducing Implications of Nanotechnology. *ACS Nano* **2008,** *2*, 395–402.
46. Nel, A.; Xia, T.; Madler, L.; Li, N. Toxic Potential of Materials at the Nanolevel. *Science* **2006,** *311*, 622–627.
47. Sager, T. M.; Porter, D. W.; Robinson, V. A.; Lindsley, W. G.; Schwegler-Berry, D. E.; Castranova, V. Improved Method To Disperse Nanoparticles for *In Vitro* and *In Vivo* Investigation of Toxicity. *Nanotoxicology* **2007,** *1*, 118–129.
48. Xia, T.; Kovochich, M.; Brant, J.; Hotze, M.; Sempf, J.; Oberley, T.; Sioutas, C.; Yeh, J. I.; Wiesner, M. R.; Nel, A. E. Comparison of the Abilities of Ambient and Manufactured Nanoparticles To Induce Cellular Toxicity According to an Oxidative Stress Paradigm. *Nano Lett.* **2006,** *6*, 1794–1807.
49. Livak, K. J.; Schmittgen, T. D. Analysis of Relative Gene Expression Data Using Real-Time Quantitative PCR and the $2(-\Delta\Delta C(t))$ Method. *Methods* **2001,** *25*, 402–408.
50. Shvedova, A. A.; Kisin, E.; Murray, A. R.; Johnson, V. J.; Gorelik, O.; Arepalli, S.; Hubbs, A. F.; Mercer, R. R.; Keohavong, P.; Sussman, N.;*et al.*Inhalation *vs.* Aspiration of Single-Walled Carbon Nanotubes in C57BL/6 Mice: Inflammation, Fibrosis, Oxidative Stress, and Mutagenesis. *Am. J. Physiol. Lung Cell Mol. Physiol.* **2008,** *295*, L552–565.
51. Li, N.; Wang, M.; Bramble, L. A.; Schmitz, D. A.; Schauer, J. J.; Sioutas, C.; Harkema, J. R.; Nel, A. E. The Adjuvant Effect of Ambient Particulate Matter Is Closely Reflected by the Particulate Oxidant Potential. *Environ. Health Perspect.* **2009,** *117*, 1116–1123.